Boomerang mechanism explaining the excess radio background

P. S. Bhupal Dev,[1, *] Pasquale Di Bari,[2, †] Ivan Martinez-Soler,[3, ‡] and Rishav Roshan[2, §]

[1]*Department of Physics and McDonnell Center for the Space Sciences,*
Washington University, St. Louis, Missouri 63130, USA
[2]*School of Physics and Astronomy, University of Southampton, Southampton, SO17 1BJ, U.K.*
[3]*Institute for Particle Physics Phenomenology, Department of Physics, Durham University, Durham DH1 3LE, U.K.*
(Dated: September 4, 2025)

We propose a *boomerang mechanism* for the explanation of the excess radio background detected by ARCADE. In an early stage, at a temperature $T \sim 100\,\mathrm{keV}$, a fraction of relic neutrinos is resonantly converted into dark neutrinos by mixing induced by a pre-existing lepton asymmetry. Dark neutrinos decay much later into a dark photon, mixed with photon, and a dark fermion, with a lifetime longer than the age of the Universe, as required by a solution to the excess radio background. This scenario circumvents the upper bound on the neutrino magnetic moment but still implies a testable lower bound.

Introduction. The Absolute Radiometer for Cosmology, Astrophysics and Diffuse Emission (ARCADE) [1] has detected an excess radio background (ERB) in the 3–10 GHz frequency range with respect to the Cosmic Microwave Background (CMB) thermal spectrum. The excess is statistically significant (more than 5σ) and cannot be explained by known population of sources since they give a contribution to the effective temperature that is 3–10 times smaller than the measured one [2]. Moreover, different observations place a strong upper limit on the anisotropy of the ERB that is, therefore, extremely smooth [3]. This represents a strong constraint for an astrophysical origin and, therefore, the ERB is currently regarded as a mystery [2]. The Tenerife Microwave Spectrometer (TMS) will soon take data in the 10–20 GHz frequency range [4, 5] and might, therefore, help to shed light on this mystery. It was noticed that radiative relic neutrino decay can potentially explain the ARCADE excess [6]. Recently, we have shown that such a solution indeed fits very well the six ARCADE data points between 3–10 GHz giving rise to an excess [7]. It predicts an effective (radiometric) temperature for the non-thermal photons produced by the decays of one of the relic neutrino species, given by

$$T_{\gamma_{\mathrm{nth}}}(E, 0) \simeq \frac{6\,\zeta(3)}{11\,\sqrt{\Omega_{\mathrm{M0}}}}\,\frac{T_0^3}{E^{1/2}\,\Delta m_1^{3/2}}\,\frac{t_0}{\tau_1}\,\left(1 + \frac{a_{\mathrm{D}}^3}{a_{\mathrm{eq}}^3}\right)^{-\frac{1}{2}},$$
(1)

where $t_0 = 4.35 \times 10^{17}\,\mathrm{s}$ is the age of the Universe, $T_0 = (2.725 \pm 0.001)\mathrm{K}$ is the photon temperature at the present time measured by the Far Infrared Absolute Spectrophotometer (FIRAS) instrument [8], $\Delta m_1 \equiv m_1 - m_0 \ll m_1$ is the mass difference between the lightest active neutrino and the new sterile state, τ_1 is the neutrino lifetime, $E \leq \Delta m_1$ is the energy of the photon at the present time. For the definition and values of the other cosmological parameters in Eq. (1), we refer the reader to Ref. [7]. This expression can be used to fit the six data points measured by ARCADE 2 in the 3–10 GHz frequency range. The best fit is obtained for $\Delta m_1 \simeq 4.0 \times 10^{-5}\,\mathrm{eV}$ and $\tau_1 \simeq$
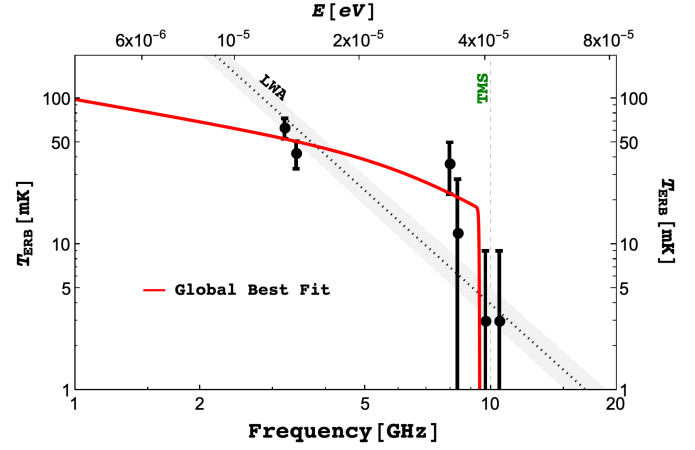

FIG. 1. Best fit curve for T_{ERB} obtained with Eq. (1). The thick red curve corresponds to the best global fit obtained for $\Delta m_1 = 4.0 \times 10^{-5}\,\mathrm{eV}$ and $\tau_1 = 1.46 \times 10^{21}\,\mathrm{s}$. The ARCADE 2 data points are taken from Ref. [1]. We also show the power-law fit $\beta = -2.58 \pm 0.05$ (dotted line with grey shade), obtained using the Long Wavelength Array (LWA) data at lower frequencies [9]. The vertical dashed line shows the TMS frequency threshold.

$1.46 \times 10^{21}\,\mathrm{s}$. As shown in Fig. 1, it provides an excellent fit to the ERB temperature spectrum over a power-law fit with $\chi^2/\mathrm{d.o.f.} \simeq 1$ with 4 degrees of freedom (d.o.f.) [7]. The result of the fit, expressed in terms of the quantity $\Delta m_1^{3/2}\tau_1$, gives at 99% confidence level (C.L.):

$$(\Delta m_1^{3/2}\tau_1)^{\mathrm{ARCADE}} = 3.8^{+7.2}_{-1.5} \times 10^{14}\,\mathrm{eV}^{3/2}\,\mathrm{s}\,.$$
(2)

This region is shown in Fig. 2 (blue patched regions with different shades for different frequency bands) in the plane Δm_1 vs. τ_1, with the best-fit point indicated by an orange ⋆.

In a general way, we can write the radiative decay rate of the neutrino mass eigenstate ν_1 with mass m_1 into another neutrino mass eigenstate ν_0 with mass m_0 in terms of the *effective magnetic transition dipole moment*
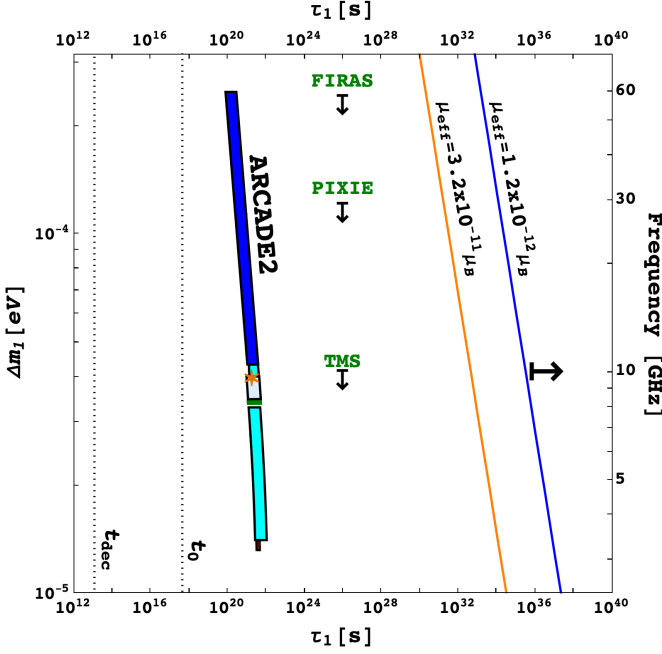
FIG. 2. Allowed region explaining the ARCADE 2 excess radio background (blue patches of different shades for different photon energy bands) [7] in the plane of Δm_1 vs. τ_1. Lower bounds on the lifetime derived from the upper bound on the effective magnetic transition dipole moment [cf. Eq. (3)] are shown by the blue and orange lines. We also indicate the matter-radiation decoupling time $t_{\rm dec}$ and the current age of the Universe t_0. The lowest frequency thresholds for FIRAS, PIXIE and TMS are also indicated.

$\mu_{\rm eff}$, as [10]

$$
\Gamma_{\nu_1 \to \nu_0 + \gamma} = \frac{(m_1^2 - m_0^2)^3}{8\pi\, m_1^3}\, \mu_{\rm eff}^2 \simeq \frac{\Delta m_1^3}{\pi}\, \mu_{\rm eff}^2 \tag{3}
$$

$$
\simeq 42.5\,{\rm s}^{-1} \left(\frac{m_1 - m_0}{\rm eV}\right)^3 \left(\frac{\mu_{\rm eff}}{\mu_{\rm B}}\right)^2 .
$$

In the second expression we used $m_1 + m_0 \simeq 2\, m_1$, since we are interested in the case of quasi-degenerate neutrinos. In the numerical expression we normalised $\mu_{\rm eff}$ to the Bohr magneton $\mu_{\rm B} = e\hbar/(2m_e) \simeq 296.3\,{\rm GeV}^{-1}$. The effective magnetic transition dipole moment is defined as

$$
\mu_{\rm eff} \equiv \sqrt{|\mu_{1\to0}|^2 + |\epsilon_{1\to0}|^2}, \tag{4}
$$

where $\mu_{1\to0}$ is the transition magnetic dipole and $\epsilon_{1\to0}$ is the transition electric dipole moment. The most stringent upper bound on $\mu_{\rm eff}$ comes from plasmon decays in globular cluster stars [11, 12]:

$$
\mu_{\rm eff} \lesssim 1.2 \times 10^{-12}\, \mu_{\rm B}. \tag{5}
$$

In this case, from Eq. (3), one easily finds the following lower bound on the lifetime of ν_1:

$$
\tau_{\nu_1 \to \nu_0 + \gamma} \gtrsim 2.5 \times 10^{21}\,{\rm s} \left(\frac{\rm eV}{\Delta m_1}\right)^3 . \tag{6}
$$

One can see that for $\Delta m_1 \lesssim 10^{-4}\,{\rm eV}$, a necessary condition to address the ERB, one obtains $\tau_{\nu_1 \to \nu_0 + \gamma} \gtrsim 10^{33}\,{\rm s}$, an incredibly long lifetime yielding completely negligible contribution to explain the ERB. This conclusion remains valid even considering the less stringent laboratory upper bound from the GEMMA experiment measuring electron recoils induced by neutrino-electron elastic scattering [13],

$$
\mu_{\rm eff} \lesssim 3.2 \times 10^{-11}\, \mu_{\rm B} . \tag{7}
$$

This situation is depicted in Fig. 2. Therefore, independently irrespective of whether the final neutrino is an active or a sterile neutrino species, neutrino radiative decay by itself cannot give any sizable contribution to explain the ERB.

The *boomerang mechanism* that we propose here provides a way to circumvent this bound, preserving at the same time the success of Eq. (1) in reproducing the ARCADE data. While in radiative neutrino decays, ordinary neutrinos directly decay into photons, in the boomerang mechanism neutrinos are first converted into dark (sterile) neutrinos and then these decay into an admixture of dark photon and photons, with the latter constituting the ERB[14]. We first discuss how active-dark neutrino mixing, in the presence of a sufficiently large lepton asymmetry, can convert a fraction of relic neutrinos into (quasi-degenerate) dark neutrinos. Second, we discuss how the dark neutrinos decay into a dark fermion species and into an admixture of photons and dark photons. Third, we combine together all constraints and determine an allowed region in the plane of the neutrino effective magnetic moment and resonance temperature that maps into a corresponding region into the plane of active-dark neutrino mixing angle versus mass squared difference. Finally, we draw some final remarks.

Active-to-dark neutrino conversions in the early Universe. We assume the existence of a light sterile dark neutrino field almost coinciding with mass eigenstate ν_0 with mass m_0 and quasi-degenerate with the lightest neutrino with positive $\Delta m^2 \equiv m_1^2 - m_0^2$ [15]. We also assume, for definiteness, that it just mixes with the muon neutrino but all results are valid in general. The much higher values of $m_{2,3}^2 - m_0^2$ make in a way that the relevant mixing parameters in vacuum are just Δm^2 and a very small muon-dark neutrino mixing angle θ_0. With these assumptions and definitions the mixing in the early Universe is described by the effective Hamiltonian ΔH that in the interaction basis can be written as

$$
\Delta H_{\mu-\rm dark} = \tag{8}
$$
$$
\frac{\Delta m^2}{4\,p} \begin{pmatrix} \cos 2\theta_0 - v(y, T_\nu, L) & -\sin 2\theta_0 \\ -\sin 2\theta_0 & -(\cos 2\theta_0 - v(y, T_\nu, L)) \end{pmatrix},
$$

where we introduced the dimensionless effective potential

$$
v(y, T, L) = v_1(y, T_\nu) + v_2(y, T_\nu, L). \tag{9}
$$

In this expression we denoted by T_ν the neutrino temperature, $y \equiv p/T_\nu$ and by L the effective (muonic) total asymmetry defined as

$$L \equiv 2L_{\nu_\mu} + L_{\nu_e} + L_{\nu_\tau} - \frac{1}{2}B_n \, , \qquad (10)$$

where the neutrino asymmetries $L_{\nu_\alpha} \equiv (N_{\nu_\alpha} - N_{\bar{\nu}_\alpha})/N_\gamma^i$ and similarly for the neutron asymmetry B_n, with N_γ^i the photon abundance at some initial time t_i such that $m_\mu \gg T_i \gg m_e$, with $T_i \equiv T(t_i)$. The term $v_1(y,T_\nu)$ is the finite temperature contribution [16] and is given by

$$v_1(y,T_\nu) = \frac{\mathrm{eV}^2}{\Delta m^2}\left(\frac{T_\nu}{T_\alpha}\right)^6 y^2 \, , \qquad (11)$$

where $T_\mu \simeq 23.4\,\mathrm{MeV}$. For $L = 0$ and $\Delta m^2 > 0$, there would be a resonance, both for neutrinos and antineutrinos, at $T_\nu^{\mathrm{res}}(y,0) \simeq T_\alpha\,(y^2\,\Delta m^2/\mathrm{eV}^2)^{1/6}$. At this resonance relic neutrinos are not efficiently converted into dark neutrinos, though this could be used to trigger the generation of a large lepton asymmetry [17, 18], as we comment in the final remarks. However, here we assume that there already exists an initial pre-existing effective muon asymmetry L_i. In this case one has also to consider the term $v_2(y,T_\nu,L)$ given by [19]

$$v_2(y,T_\nu,L) \simeq \mp v_0\,\frac{\mathrm{eV}^2}{\Delta m^2}\,L\left(\frac{T_\nu}{\mathrm{MeV}}\right)^4 y \, , \qquad (12)$$

where the $-$ $(+)$ sign holds for neutrinos (antineutrinos) and $v_0 = (4\sqrt{2}\zeta(3)/\pi^2)10^{12}\,G_F\mathrm{MeV}^2 \simeq 8$. If we assume that $|L_i| \gg L_\star \simeq 0.4 \times 10^{-6}(y\,\Delta m^2/\mathrm{eV}^2)^{1/3}$, then the resonance condition is satisfied for $v_2(y,T_\nu,L) = 1$. This implies that for positive L_i and positive Δm^2 there is a resonance only for antineutrinos at a resonant temperature

$$T_\nu^{\mathrm{res}}(y,L \gg L_\star) = \left(\frac{1}{v_0\,L\,y}\frac{\Delta m^2}{\mathrm{eV}^2}\right)^{\frac{1}{4}}\mathrm{MeV} < T_\nu^{\mathrm{res}}(y,0) \, . \qquad (13)$$

Notice that this resonance occurs at different times for different values of $y = y_{\mathrm{res}}$. The asymmetry grows with time from the initial value and y_{res} spans all neutrino distribution starting from a small value $y_{\mathrm{res}} \ll 1$ to large values $y_{\mathrm{res}} \gg 1$, as discussed in detail in Ref. [18]. Since this process occurs, in general, during electron-positron annihilations, the neutrino temperature get smaller than the photon temperature and, making use of entropy conservation, one has

$$T_\nu = T\left[\frac{g_S(m_e/T)}{g_S(0)}\right]^{\frac{1}{3}} \, , \qquad (14)$$

where g_S is the number of entropy density ultrarelativistic degrees of freedom. For $T_\nu^{\mathrm{res}}(y_{\mathrm{res}} \ll 1, L_i) \lesssim 1\,\mathrm{MeV}$, neutrino collisions can be neglected and at the resonance

one has antineutrino conversions into dark neutrinos already starting from small $y_{\mathrm{res}} \ll 1$. If the resonance is crossed adiabatically, then all lightest antineutrinos are converted into dark neutrinos. Notice that if $L_i < 0$, then simply lightest neutrinos are converted into dark neutrinos instead of antineutrinos. For definiteness, we will usually refer to the case $L_i > 0$ in the following. More generally, to account also for non-adiabatic conversions, the fraction of converted neutrinos can be calculated using the Landau-Zener approximation that has been shown to agree quite well with numerical results solving density matrix equation [18]:

$$f_{\nu_\mu \to \nu_{\mathrm{dark}}} \simeq 1 - e^{-\frac{\pi}{2}\gamma_{\mathrm{res}}} \, , \qquad (15)$$

where γ_{res} is the adiabaticity parameter at the resonance and is given by

$$\gamma_{\mathrm{res}} = \frac{|\Delta m^2|\,\sin^2 2\theta_0}{2y\,T_\nu^{\mathrm{res}}\,H_{\mathrm{res}}} \, , \qquad (16)$$

where $H_{\mathrm{res}} \simeq 0.2\mathrm{s}^{-1}\sqrt{g_\rho(T_{\mathrm{res}})}(T_{\mathrm{res}}/\mathrm{MeV})^2$ is the expansion rate at the resonance and g_ρ is the number of energy density ultrarelativistic degrees of freedom. For simplicity, we can make use of a monochromatic approximation equivalent to say that all neutrinos are converted instantaneously at T_ν^{res} corresponding at $y_{\mathrm{res}} = 3.15$. Using the prescription in Ref. [18], in this case one has to use $\langle L \rangle \simeq L_f/2 \simeq 0.2$ in the evaluation of the adiabaticity parameter, obtaining:

$$\gamma_{\mathrm{res}} \simeq 1.4 \times 10^9\,\sqrt{\frac{10.75}{g_\rho(T_\nu^{\mathrm{res}})}}\left(\frac{\Delta m^2}{\mathrm{eV}^2}\right)^{\frac{1}{4}}\sin^2 2\theta_0 \, . \qquad (17)$$

We will comment in the final remarks on the validity of the monochromatic approximation.

Dark neutrino decays into a dark-standard photon admixture. In order to explain the ERB, we assume that the dark neutrinos produced by active-to-dark neutrino conversions in the presence of a pre-existing asymmetry decay into a dark fermion ψ' with mass $m_{\psi'}$ and a dark photon γ' with mass $m_{\gamma'}$ kinematically mixed with the standard photon with kinetic mixing parameter $\varepsilon = \sin^2\chi_0$. The dark fermion is assumed to be quasi-degenerate with ν_0, while we assume $m_{\gamma'} \lesssim 10^{-16}\,\mathrm{eV}$, in a way to evade any constraint for all values of ε [20]. We also assume that the decays can be described as fully non-relativistically so that, at the decay, the dark-standard photon admixture has an energy $E_D \simeq \Delta m' \equiv m_0 - m_{\psi'}$. In this way the spectrum of non-thermal photons produced by the decays of the dark neutrinos and detected at the present time would be described by an effective temperature given exactly by the expression in Eq. (1) multiplied by ε and also divided by a factor $2/(1 - e^{-\frac{\pi}{2}\gamma_{\mathrm{res}}})$, taking into account that only relic antineutrinos are, adiabatically or non-adiabatically, converted into dark neutrinos.

The dark fermion radiative decay rate into a dark photon can be related to a dark neutrino effective magnetic moment $\mu'_{\rm eff}$ by an expression analogous to Eq. (3) [21]:

$$\Gamma_{\nu_0 \to \psi' + \gamma'} = \frac{(m_0^2 - m_{\psi'}^2)^3}{8\pi \, m_0^3} \, \mu'^2_{\rm eff} \simeq \frac{\Delta m'^3}{\pi} \, \mu'^2_{\rm eff}$$

$$\simeq 42.5\,{\rm s}^{-1} \left(\frac{\Delta m'}{\rm eV}\right)^3 \left(\frac{\mu'_{\rm eff}}{\mu_{\rm B}}\right)^2 . \quad (18)$$

The important difference is that now $\mu'_{\rm eff}$ does not have direct experimental constraints. However, because of the active-dark neutrino mixing, the active neutrino still has an effective neutrino magnetic moment $\mu_{\rm eff} = \sin^2\theta_0 \mu'_{\rm eff}$ and for this reason the experimental constraints on $\mu_{\rm eff}$ still play a role to be taken into account.

Constraints and allowed region. Let us now combine all constraints and determine the allowed region in the space of parameters. Of course we have first to determine which is a minimum set of parameters to show all constraints. We can start by imposing that the non-thermal photons produced by the decays of the dark neutrinos, and mixed with the dark photons, can reproduce the ARCADE data. We have then to impose that the lifetime of dark neutrinos is given by the lifetime determined in [7] in the case of direct relic neutrino decays (see best fit in Fig. 1), that we denote by $\tau_{\rm ARCADE}(\nu_1 \to \nu_0 + \gamma)$, shortened by a factor $\varepsilon\,(1 - e^{-\gamma_{\rm res}})/2$ to compensate the reduced photon production, explicitly:

$$\tau_{\nu_0 \to \psi' + \gamma'} = \frac{\varepsilon\,(1 - e^{-\gamma_{\rm res}})}{2} \tau_{\rm ARCADE}(\nu_1 \to \nu_0 + \gamma) \gtrsim t_0 . \quad (19)$$

On the other hand, the lifetime cannot be shorter than t_0, as also indicated in (19), since otherwise the exponential in the decay-law kicks in and suppresses the photon effective temperature below the ARCADE measured values. Since the lifetime is the inverse of the decay rate given in Eq. (3), it is clear that the constraint (19) allows to express $\mu'_{\rm eff}$ in terms of $\gamma_{\rm res}$. Therefore, for a fixed value of $\gamma_{\rm res}$, one has a fixed value of $\mu'_{\rm eff}$. At the same time $\gamma_{\rm res}$ is expressed in terms of $\sin^2 2\theta_0$ and Δm^2 from Eq. (17).

We also have to impose the constraint $T_\nu^{\rm res}(L_{\rm i}) \lesssim 1\,{\rm MeV}$. From Eq. (13) one can see that, for a fixed value of $L_{\rm i}$, this results into an upper bound on Δm^2. Higher values of $L_{\rm i}$ correspond to higher allowed values of Δm^2. However, one has to impose an upper bound $L_{\rm i} \lesssim 10^{-2}$ from cosmological observations, since this would affect both BBN and CMB anisotropies [22]. It is then clear that it is possible to express all other parameters in terms of $\sin^2 2\theta_0$, Δm^2 and $L_{\rm i}$. Therefore, we can conveniently show all constraints in the plane Δm^2 versus $\sin^2 2\theta_0$, as one can see in the left panel of Fig. 3 for the most conservative choice of maximal kinetic mixing corresponding to $\varepsilon = 1/2$ and highest value of $\tau_{\rm ARCADE}(\nu_1 \to \nu_0 + \gamma)$ allowed at 99% C.L. (from Eq. (2)). All constraints are ex-

plicitly indicated and the allowed region is in white. The horizontal dashed lines give the upper bound on Δm^2 for different values of $L_{\rm i}$. One can also notice the experimental constraints on $\mu_{\rm eff}$ that basically translates into an upper bound on $\sin^2 2\theta_0$. The orange line is the iso-contour line for $\gamma_{\rm res} = 1$, marking the border between the adiabatic and the non-adiabatic regime. In the right panel of Fig. 3 we also show constraints and allowed region in the plane $\mu_{\rm eff}$ versus $T_\nu^{\rm res}$ and one can see how there is a very interesting lower bound $\mu_{\rm eff}/\mu_{\rm B} \gtrsim 10^{-16}$.

Final remarks. (i) The boomerang mechanism effectively realizes a solution of the ERB mystery obtained in terms of radiative relic neutrino decays [7] but in two stages: in a first early stage relic antineutrinos (or neutrinos, depending on the sign of $L_{\rm i}$) of one species are converted into dark neutrinos (the visible sector throws particles into the dark sector); in a second stage dark neutrinos decay into dark photons mixed with photons (dark sector throws back particles into the visible one). (ii) As Fig. 3 shows, it has a broad variety of phenomenological implications that make it testable in different ways. First of all the TMS experiment will verify the ARCADE data, the existence of the ERB and the solution proposed in [7]. Notice also that this implies some non-standard deviation in the 21 cm cosmological global signal (see [7] for details). Possible cosmological anomalies in BBN and/or CMB anisotropies might be addressed by the presence of a large lepton asymmetry [23]. Also notice that it implies non-standard relic neutrino background properties that might be potential measured [18]. Finally, the lower bound we found on $\mu_{\rm eff}$, four orders of magnitude below the current upper bound, will be tested by future experiments [24]. (iii) The initial lepton asymmetry $L_{\rm i}$ can either be generated by some external mechanism, such as the decays of weakly coupled seesaw neutrinos, or, even more intriguingly, it could be generated dynamically by the same active-dark neutrino mixing [17, 18]. In this case, for $L = 0$, the initial resonance at $T_\nu^{\rm res}(0) \gtrsim 1\,{\rm MeV}$ occurs in the collisional regime and triggers an initial unstable growth of the asymmetry. This stage would then provide the value we denoted by $L_{\rm i}$ needed for the conversion of active to dark neutrinos. This option might require a reduced allowed region in the plane Δm^2 versus $\sin^2 2\theta_0$. (iv) The monochromatic approximation we used is well justified by numerical solution of density matrix equation with a full momentum description [18]. This also grasps the variation of the non-adiabaticity parameter with momentum. However, one would have small corrections to the allowed region we have derived. (v) That allowed regions have been determined for the most conservative case $\varepsilon = 1/2$. They would clearly shrink for lower values until they would disappear for a lower bound $\varepsilon \sim 2 \times 10^{-4}$. (vi) We have not discussed how the boomerang mechanism could be embedded within a full model. For example, a possible direction is offered by models incorporating quasi-
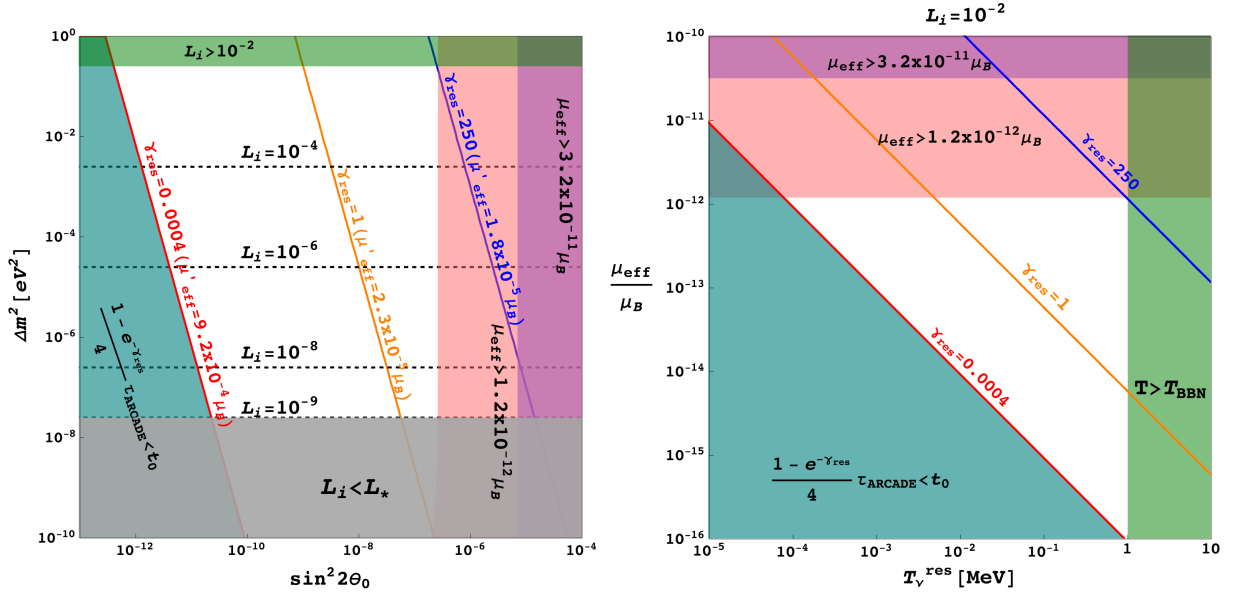
FIG. 3. Left panel: Constraints (shaded) and allowed region (white) in the plane of Δm^2 versus $\sin^2 2\theta_0$. The horizontal dashed lines give an upper bound on Δm^2 from $T_\nu^{\rm res} < 1\,{\rm MeV}$ for the indicated values of $L_{\rm i}$. Right panel: Constraints (shaded) and allowed region (white) in the plane of $\mu_{\rm eff}$ versus $T_\nu^{\rm res}$. We have used conservatively maximal kinetic mixing $\varepsilon = 1/2$.

Dirac neutrinos. Typically, we have maximal mixing for $\Delta m \ll m$, as $\tan 2\theta \sim 2m/\Delta m$, but arbitrary mixing is possible for a matrix structure.

In conclusion, the boomerang mechanism shows that a solution to the ERB in terms of relic radiative neutrino decays is possible. If the excess will be confirmed, this might provide a direct open window to explore a new dark sector.

Acknowledgments. We thank Jens Chluba, André de Gouvêa, Chee Sheng Fong, Josè Alberto Rubiño Martin, and Anil Thapa for useful discussions. The work of BD was partly supported by the U.S. Department of Energy under grant No. DE-SC0017987. PDB and RR acknowledge financial support from the STFC Consolidated Grant ST/T000775/1. IMS is supported by STFC grant ST/T001011/1.

APPENDIX: BOOMERANG MECHANISM VERSUS NEUTRINO OSCILLATION CONSTRAINTS

Having obtained an allowed region in the Δm^2 versus $\sin^2 2\theta$ plane, we compare it with the existing constraints from neutrino oscillation experiments. Active research is underway on sterile neutrinos with masses around the eV scale, motivated by the excess observed by LSND [25], and the intriguing results reported by MiniBooNE [26], BEST [27], and IceCube [28]. However, many other experiments have not found such evidence, leading to significant tension among data sets when combined [29, 30].

Beyond the eV-scale sterile neutrino, searches have explored a wide range of mass for oscillations between active and sterile states [31–42], but no evidence has been found. For nearly degenerate active and sterile states, solar [36, 43, 44], and reactor data [45], constrain $\Delta m^2 \lesssim 10^{-12}{\rm eV}^2$ and $\sin^2 2\theta \geq 10^{-4}$, as shown in Fig. 4. The disappearance bounds of muons come from long-baseline experiments [46, 47] and atmospheric experiments [48], $\Delta m^2 \lesssim 10^{-4}$ eV^2 and $\sin^2 2\theta \geq 10^{-2}$. Astrophysical neutrinos, with large L/E, probe down to $\Delta m^2 \sim 10^{-20}{\rm eV}^2$ for maximal mixing [40, 49–51].

Fig. 4 compares current bounds with the region predicted by the boomerang mechanism. While this work focuses on muon-sterile oscillations, the mechanism applies to all flavors, so we used the strongest bounds over the mixing. Upcoming experiments like DARWIN [50] and JUNO [52] will further improve sensitivity.

———

* bdev@wustl.edu
† P.Di-Bari@soton.ac.uk
‡ ivan.j.martinez-soler@durham.ac.uk
§ roshan@soton.ac.uk

[1] D. J. Fixsen *et al.*, ARCADE 2 Measurement of the Extra-Galactic Sky Temperature at 3-90 GHz, Astrophys. J. **734**, 5 (2011), arXiv:0901.0555 [astro-ph.CO].

[2] J. Singal *et al.*, The Radio Synchrotron Background: Conference Summary and Report, Publ. Astron. Soc. Pac. **130**, 036001 (2018), arXiv:1711.09979 [astro-ph.HE].

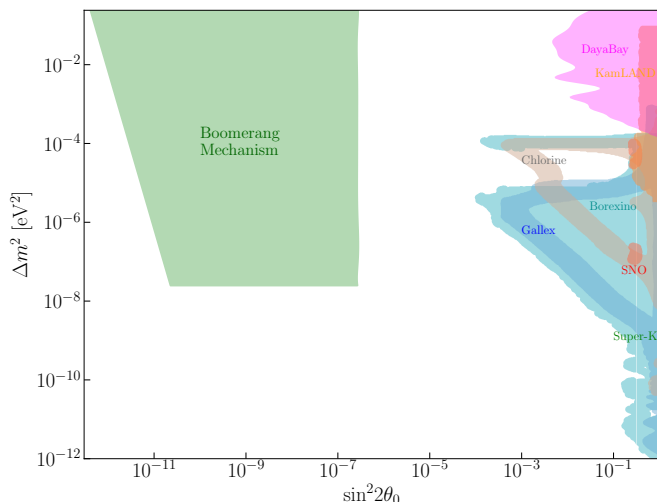[3] G. P. Holder, The unusual smoothness of the extragalac-

FIG. 4. Region allowed by the boomerang mechanism at 99% C.L., along with the region excluded by oscillation experiments. We present some of the most stringent bounds on the mixing, including measurements from solar neutrino experiments such as Borexino [44], Gallex [53], Chlorine [54], and SNO [55], Super-Kamiokande [56] as well as reactor experiments like KamLAND [44] and Daya Bay [45].

tic unresolved radio background, Astrophys. J. **780**, 112 (2014), arXiv:1207.0856 [astro-ph.CO].

[4] J. A. Rubiño Martín *et al.*, The Tenerife Microwave Spectrometer (TMS) experiment: studying the absolute spectrum of the sky emission in the 10-20GHz range, in *Millimeter, Submillimeter, and Far-Infrared Detectors and Instrumentation for Astronomy X*, Society of Photo-Optical Instrumentation Engineers (SPIE) Conference Series, Vol. 11453, edited by J. Zmuidzinas and J.-R. Gao (2020) p. 114530T.

[5] P. Alonso-Arias, P. A. Fuerte-Rodríguez, R. J. Hoyland, and J. A. Rubiño-Martín, The optical system of the Tenerife Microwave Spectrometer: a window for observing the 10–20 GHz sky spectra, JINST **16** (12), P12037, arXiv:2111.15364 [astro-ph.IM].

[6] M. Chianese, P. Di Bari, K. Farrag, and R. Samanta, Probing relic neutrino radiative decays with 21 cm cosmology, Phys. Lett. B **790**, 64 (2019), arXiv:1805.11717 [hep-ph].

[7] P. S. B. Dev, P. Di Bari, I. Martínez-Soler, and R. Roshan, Relic neutrino decay solution to the excess radio background, JCAP **04**, 046, arXiv:2312.03082 [hep-ph].

[8] D. J. Fixsen, The Temperature of the Cosmic Microwave Background, Astrophys. J. **707**, 916 (2009), arXiv:0911.1955 [astro-ph.CO].

[9] J. Dowell and G. B. Taylor, The Radio Background Below 100 MHz, Astrophys. J. Lett. **858**, L9 (2018), arXiv:1804.08581 [astro-ph.CO].

[10] Z.-z. Xing and S. Zhou, *Neutrinos in particle physics, astronomy and cosmology* (2011).

[11] G. G. Raffelt, New bound on neutrino dipole moments from globular cluster stars, Phys. Rev. Lett. **64**, 2856 (1990).

[12] F. Capozzi and G. Raffelt, Axion and neutrino bounds

[13] improved with new calibrations of the tip of the red-giant branch using geometric distance determinations, Phys. Rev. D **102**, 083007 (2020), arXiv:2007.03694 [astro-ph.SR].

[13] A. G. Beda, V. B. Brudanin, V. G. Egorov, D. V. Medvedev, V. S. Pogosov, M. V. Shirchenko, and A. S. Starostin, Upper limit on the neutrino magnetic moment from three years of data from the GEMMA spectrometer, (2010), arXiv:1005.2736 [hep-ex].

[14] The name boomerang scenario is because the visible sector first throws sterile neutrinos into the dark sector via mixing, and then these, decaying, throw back photons into the visible sector. The net result is that neutrinos are converted into photons. Trading off the effective magnetic moment of ordinary neutrinos with that of sterile neutrino to circumvent (5) is an ingredient, the only one, in common with the model proposed in [**?**] to explain the EDGES anomaly.

[15] We adopt a different sign convention for Δm^2 than in [18, 19].

[16] D. Nötzold and G. Raffelt, Neutrino dispersion at finite temperature and density, Nucl. Phys. B **307**, 924 (1988).

[17] R. Foot, M. J. Thomson, and R. R. Volkas, Large neutrino asymmetries from neutrino oscillations, Phys. Rev. D **53**, R5349 (1996), arXiv:hep-ph/9509327.

[18] P. Di Bari and R. Foot, Active sterile neutrino oscillations in the early universe: Asymmetry generation at low —delta m**2— and the Landau-Zener approximation, Phys. Rev. D **65**, 045003 (2002), arXiv:hep-ph/0103192.

[19] K. Enqvist, K. Kainulainen, and J. Maalampi, Refraction and Oscillations of Neutrinos in the Early Universe, Nucl. Phys. B **349**, 754 (1991).

[20] A. Caputo, A. J. Millar, C. A. J. O'Hare, and E. Vitagliano, Dark photon limits: A handbook, Phys. Rev. D **104**, 095029 (2021), arXiv:2105.04565 [hep-ph].

[21] This ingredient of the mechanism is in common with the model proposed in [**?**] to explain the EDGES anomaly.

[22] A. D. Dolgov, S. H. Hansen, S. Pastor, S. T. Petcov, G. G. Raffelt, and D. V. Semikoz, Cosmological bounds on neutrino degeneracy improved by flavor oscillations, Nucl. Phys. B **632**, 363 (2002), arXiv:hep-ph/0201287.

[23] A.-K. Burns, T. M. P. Tait, and M. Valli, Indications for a Nonzero Lepton Asymmetry from Extremely Metal-Poor Galaxies, Phys. Rev. Lett. **130**, 131001 (2023), arXiv:2206.00693 [hep-ph].

[24] C. Giunti, K. Kouzakov, Y.-F. Li, and A. Studenikin, Neutrino Electromagnetic Properties 10.1146/annurev-nucl-102122-023242 (2024), arXiv:2411.03122 [hep-ph].

[25] A. Aguilar *et al.* (LSND), Evidence for neutrino oscillations from the observation of $\bar{\nu}_e$ appearance in a $\bar{\nu}_\mu$ beam, Phys. Rev. D **64**, 112007 (2001), arXiv:hep-ex/0104049.

[26] A. A. Aguilar-Arevalo *et al.* (MiniBooNE), Updated MiniBooNE neutrino oscillation results with increased data and new background studies, Phys. Rev. D **103**, 052002 (2021), arXiv:2006.16883 [hep-ex].

[27] V. V. Barinov *et al.*, Results from the Baksan Experiment on Sterile Transitions (BEST), Phys. Rev. Lett. **128**, 232501 (2022), arXiv:2109.11482 [nucl-ex].

[28] R. Abbasi *et al.* ((IceCube Collaboration)‖, IceCube), Search for an eV-Scale Sterile Neutrino Using Improved High-Energy $\nu\mu$ Event Reconstruction in IceCube, Phys. Rev. Lett. **133**, 201804 (2024), arXiv:2405.08070 [hep-ex].

[29] M. Dentler, Á. Hernández-Cabezudo, J. Kopp, P. A. N. Machado, M. Maltoni, I. Martinez-Soler, and T. Schwetz, Updated Global Analysis of Neutrino Oscillations in the Presence of eV-Scale Sterile Neutrinos, JHEP **08**, 010, arXiv:1803.10661 [hep-ph].

[30] J. M. Hardin, I. Martinez-Soler, A. Diaz, M. Jin, N. W. Kamp, C. A. Argüelles, J. M. Conrad, and M. H. Shaevitz, New Clues about light sterile neutrinos: preference for models with damping effects in global fits, JHEP **09**, 058, arXiv:2211.02610 [hep-ph].

[31] L. Wolfenstein, Different Varieties of Massive Dirac Neutrinos, Nucl. Phys. B **186**, 147 (1981).

[32] S. T. Petcov, On Pseudodirac Neutrinos, Neutrino Oscillations and Neutrinoless Double beta Decay, Phys. Lett. B **110**, 245 (1982).

[33] S. M. Bilenky and B. Pontecorvo, Neutrino Oscillations With Large Oscillation Length in Spite of Large (Majorana) Neutrino Masses?, Sov. J. Nucl. Phys. **38**, 248 (1983).

[34] M. Kobayashi and C. S. Lim, Pseudo Dirac scenario for neutrino oscillations, Phys. Rev. D **64**, 013003 (2001), arXiv:hep-ph/0012266.

[35] G. Anamiati, R. M. Fonseca, and M. Hirsch, Quasi Dirac neutrino oscillations, Phys. Rev. D **97**, 095008 (2018), arXiv:1710.06249 [hep-ph].

[36] A. de Gouvea, W.-C. Huang, and J. Jenkins, Pseudo-Dirac Neutrinos in the New Standard Model, Phys. Rev. D **80**, 073007 (2009), arXiv:0906.1611 [hep-ph].

[37] F. Vissani and A. Boeltzig, Supernova Neutrinos: Risks and Opportunities, PoS **NEUTEL2015**, 008 (2015).

[38] I. M. Shoemaker and K. Murase, Probing BSM Neutrino Physics with Flavor and Spectral Distortions: Prospects for Future High-Energy Neutrino Telescopes, Phys. Rev. D **93**, 085004 (2016), arXiv:1512.07228 [astro-ph.HE].

[39] V. Brdar and R. S. L. Hansen, IceCube Flavor Ratios with Identified Astrophysical Sources: Towards Improving New Physics Testability, JCAP **02**, 023, arXiv:1812.05541 [hep-ph].

[40] A. De Gouvêa, I. Martinez-Soler, Y. F. Perez-Gonzalez, and M. Sen, Fundamental physics with the diffuse supernova background neutrinos, Phys. Rev. D **102**, 123012 (2020), arXiv:2007.13748 [hep-ph].

[41] T. Rink and M. Sen, Constraints on pseudo-Dirac neutrinos using high-energy neutrinos from NGC 1068, Phys. Lett. B **851**, 138558 (2024), arXiv:2211.16520 [hep-ph].

[42] K. Carloni, I. Martínez-Soler, C. A. Arguelles, K. S. Babu, and P. S. B. Dev, Probing pseudo-Dirac neutrinos with astrophysical sources at IceCube, Phys. Rev. D **109**, L051702 (2024), arXiv:2212.00737 [astro-ph.HE].

[43] S. Ansarifard and Y. Farzan, Revisiting pseudo-Dirac neutrino scenario after recent solar neutrino data, Phys. Rev. D **107**, 075029 (2023), arXiv:2211.09105 [hep-ph].

[44] Z. Chen, J. Liao, J. Ling, and B. Yue, Constraining superlight sterile neutrinos at Borexino and KamLAND, JHEP **09**, 004, arXiv:2205.07574 [hep-ph].

[45] F. P. An et al. (Daya Bay), Search for a Sub-eV Sterile Neutrino using Daya Bay's Full Dataset, Phys. Rev. Lett. **133**, 051801 (2024), arXiv:2404.01687 [hep-ex].

[46] P. Adamson et al. (MINOS+), Search for sterile neutrinos in MINOS and MINOS+ using a two-detector fit, Phys. Rev. Lett. **122**, 091803 (2019), arXiv:1710.06488 [hep-ex].

[47] M. A. Acero et al. (NOvA), Dual-Baseline Search for Active-to-Sterile Neutrino Oscillations in NOvA, Phys. Rev. Lett. **134**, 081804 (2025), arXiv:2409.04553 [hep-ex].

[48] J. F. Beacom, N. F. Bell, D. Hooper, J. G. Learned, S. Pakvasa, and T. J. Weiler, PseudoDirac neutrinos: A Challenge for neutrino telescopes, Phys. Rev. Lett. **92**, 011101 (2004), arXiv:hep-ph/0307151.

[49] I. Martinez-Soler, Y. F. Perez-Gonzalez, and M. Sen, Signs of pseudo-Dirac neutrinos in SN1987A data, Phys. Rev. D **105**, 095019 (2022), arXiv:2105.12736 [hep-ph].

[50] A. de Gouvêa, E. McGinness, I. Martinez-Soler, and Y. F. Perez-Gonzalez, pp solar neutrinos at DARWIN, Phys. Rev. D **106**, 096017 (2022), arXiv:2111.02421 [hep-ph].

[51] K. Carloni, Y. Porto, C. A. Argüelles, P. S. B. Dev, and S. Jana, Signatures of quasi-Dirac neutrinos in diffuse high-energy astrophysical neutrino data, (2025), arXiv:2503.19960 [hep-ph].

[52] J. Franklin, Y. F. Perez-Gonzalez, and J. Turner, JUNO as a probe of the pseudo-Dirac nature using solar neutrinos, Phys. Rev. D **108**, 035010 (2023), arXiv:2304.05418 [hep-ph].

[53] W. Hampel et al. (GALLEX), GALLEX solar neutrino observations: Results for GALLEX IV, Phys. Lett. B **447**, 127 (1999).

[54] B. T. Cleveland, T. Daily, R. Davis, Jr., J. R. Distel, K. Lande, C. K. Lee, P. S. Wildenhain, and J. Ullman, Measurement of the solar electron neutrino flux with the Homestake chlorine detector, Astrophys. J. **496**, 505 (1998).

[55] Q. R. Ahmad et al. (SNO), Direct evidence for neutrino flavor transformation from neutral current interactions in the Sudbury Neutrino Observatory, Phys. Rev. Lett. **89**, 011301 (2002), arXiv:nucl-ex/0204008.

[56] S. Fukuda et al. (Super-Kamiokande), Solar B-8 and hep neutrino measurements from 1258 days of Super-Kamiokande data, Phys. Rev. Lett. **86**, 5651 (2001), arXiv:hep-ex/0103032.